IJRCS

International Journal of Robotics and Control Systems
Vol. 5, No. 6, 2025, pp. 2831-2852
ISSN 2775-2658
http://pubs2.ascee.org/index.php/ijrcs

ASCEE

Anti-Collision Formation Control for Drone Swarms Tracking Aerial Targets Under Wind Disturbance

Imam Barket Ghiloubi [a,1,*], Latifa Abdou [a,b,2], Oussama Lahmar [a,3]

[a] Identification, Command, Control & Communication, Mohamed Khider University, Biskra/07000, Algeria
[b] Department of Electronics, Mostefa Ben Boulaïd University, Batna/05000, Algeria
[1] imam.ghiloubi@univ-biskra.dz; [2] l.abdou@univ-batna2.dz; [3] oussama.lahmar@univ-biskra.dz
* Corresponding Author

ARTICLE INFO

Article history
Received June 12, 2025
Revised August 24, 2025
Accepted December 03, 2025

Keywords
Backstepping;
Drones Swarm;
Wind Disturbance Rejection;
Decentralized Formation Control;
Anti-Collision

ABSTRACT

Drone swarms are increasingly used for complex aerial missions requiring coordination, adaptability, and wide-area observation. This paper presents a robust decentralized formation control strategy for a group of quadrotor drones assigned to track and monitor a moving aerial target in dynamic environments. The main challenges addressed include maintaining stable coordination under wind disturbances and preventing inter-drone collisions, without relying on centralized supervision or global shape feedback. A backstepping control optimized by Flower Pollination Algorithm is proposed, where wind effects are directly integrated into the dynamics and compensated through feedforward terms. In contrast to other formation strategies, the proposed approach enables formation-level coordination using only local relative position data, facilitating decentralized implementation. Each follower drone maintains a regular pentagon formation around the target to ensure full viewing angle. While ideal sensing is assumed for the simulation, the framework is compatible with practical sensor constraints. To enhance performance, the control gains are optimized using the metaheuristic flower pollination algorithm, selected for its balance between convergence speed and global search capability. Extensive simulations demonstrate that the proposed system achieves accurate tracking, stable formation maintenance during target movement in different scenarios, effective collision avoidance, and robustness against realistic wind disturbances. Results show ≈ 0% overshoot and a settling time ranging from 1 to 2 seconds, depending on the initial and final positions of each drone in the pentagonal formation, which confirms stability and precision. This contribution bridges robust nonlinear control and fully decentralized swarm coordination, offering a scalable and resilient solution for multi-agent aerial operations.

1. Introduction

The recent rise in the deployment of Unmanned Aerial Vehicles (UAVs) in applications such as environmental monitoring, infrastructure inspection, and search and rescue missions has emphasized the need for intelligent, autonomous swarm coordination strategies. Aerial swarms offer advantages in terms of scalability and redundancy, but ensuring robust formation control, especially in dynamic

environments, remains a significant challenge. Recent advances in quadrotor control have seen the integration of adaptive backstepping combined with sliding mode control techniques to improve robustness and performance under dynamic condition [1]. Robust model reference adaptive backstepping sliding-mode controllers enhanced by disturbance observers have also been developed to maintain precise attitude control despite external perturbations [2]. To handle actuator faults effectively, fault-tolerant super twisting sliding mode control has been proposed alongside control allocation strategies for quadrotor UAVs [3]. Finite-time disturbance observers paired with adaptive nonsingular fast terminal sliding mode control have been introduced to guarantee rapid convergence and robustness in quadrotor systems [4]. Adaptive nonsingular terminal sliding mode controllers have been designed to tackle mass uncertainties and input delays, ensuring stable tracking performance [5]. Position tracking in micro aerial vehicles has benefited from adaptive PID controllers integrated with sliding mode to achieve reliable real-time performance [6].

Trajectory tracking under practical constraints such as input saturation and external disturbances has been addressed through adaptive sliding mode control algorithms specialized for quadrotor UAVs [7]. Flight stability improvements have been achieved by implementing adaptive super-twisting reaching laws within sliding mode control frameworks [8]. Further, the delta operator framework has been employed to develop adaptive sliding mode attitude controllers that enhance computational efficiency and robustness [9]. Quadrotor trajectory tracking has also been tackled via adaptive non-singular terminal sliding mode control schemes, demonstrating improved control accuracy [10]. Robust control architectures integrating uncertainty and disturbance estimators have been proposed to maintain operation even during motor failures [11]. High-gain disturbance observers have shown promise in enhancing robust trajectory tracking by effectively estimating and compensating for disturbances [12]. Adaptive fast-reaching nonsingular terminal sliding mode controllers have been developed to mitigate model uncertainties and external disturbances, ensuring precise tracking of quadrotor UAVs [13]. Several recent works have addressed the challenges of formation control in multi-quadrotor systems under realistic conditions. Robust formation control strategies have been developed to mitigate the effects of communication delays and wind disturbances [14].

Leader-follower consensus control schemes have been proposed for managing constraints in multi-agent systems [15], while adaptive control approaches aim to preserve formation under external disturbances [16]. Distributed control based on consensus algorithms has been explored to ensure coordination across large quadrotor swarms [17], and event-triggered communication mechanisms have been introduced to reduce bandwidth requirements while maintaining cooperative performance [18]. Hybrid technique combining Fuzzy Logic Control (FLC) and Proportional, Integral, and Derivative (PID) is developped in [19] for multi-UAV leader-follower control. Moreover, cooperative control frameworks have been extended to heterogeneous drone-robot interaction systems [20]. Disturbance observer-based leader-follower control has enhanced robustness in multi-agent quadrotor systems [21], and reinforcement learning has been used to develop adaptive controllers for formation in dynamic environments [22]. Fault-tolerant cooperative control solutions have been proposed to handle actuator failures [23], Along with a presentation of recent methods for fault-tolerant control in multi-UAV systems [24].

Neural network-based distributed control has also been utilized to address communication constraints [25], while consensus algorithms have been adapted to cope with time-varying communication topologies [26]. Dynamic obstacle avoidance has been achieved and integrated into leader-follower strategie [27], and robust cooperative control frameworks have further addressed both actuator faults and external perturbations [28]. Event-triggered leader-follower designs have enabled efficient communication in networks with switching topologies [29], and adaptive fault-tolerant control schemes have been developed to overcome both communication delays and actuator malfunctions [30]. In GPS-denied environments, hybrid control strategies have been developed to enable formation flying with obstacle avoidance [31], while consensus-based and distributed model predictive control (MPC) approaches have ensured precise multi-agent coordination [32]. Formation control framework is proposed for heterogeneous multi-agent systems to enhance cooperative behavior [33], and sliding mode control has shown strong disturbance rejection capabilities [34].

Nonlinear observer-based leader-follower designs have also been explored to improve formation stability [35], along with event-triggered communication strategies to reduce bandwidth usage without compromising performance [36].

Fault-tolerant control methods have been proposed to handle actuator failures and wind disturbances [37], and adaptive consensus strategies have addressed measurement noises [38]. Distributed MPC has been effectively applied for coordination in cluttered environments [39], and multiple studies have developed cooperative control algorithms under communication constraints using event-triggered and graph-based designs [40]-[42]. Collision avoidance has been achieved using barrier functions in nonlinear multi-agent control [43], while reinforcement learning has enhanced trajectory tracking under uncertain dynamics [44]. Furthermore, robust formation control incorporating adaptive observers, energy-efficient triggering mechanisms, and vision-based localization has been developed [45]-[47], along with neural network-based and predictive adaptive strategies for complex dynamic scenarios [48]-[50]. Additional contributions include vision-based relative localization with communication constraints [51], resilient fault detection in UAV swarms [52], finite-time convergence using backstepping control of multi UAV system [53], and passivity-based adaptive control of multi robot system [54].

Finite-time consensus techniques, observer-based compensators, and nonlinear adaptive controllers have been proposed for multi agent system control [55]-[57], while event-triggered sliding mode predictive control has addressed disturbance rejection [58]. Finally, reinforcement learning-assisted leader-follower control has enabled adaptive trajectory formation in changing environments [59]. Most of the well-known control strategies proposed in the literature can be categorized into linear, nonlinear, and intelligent control approaches. Linear methods such as PID and Linear Quadratic Regulator (LQR) are widely used due to their simplicity and ease of implementation, but they often show limitations when dealing with strong nonlinearities, model uncertainties, or external disturbances. Nonlinear techniques, including Sliding Mode Control (SMC) and backstepping, offer enhanced robustness and better performance in complex dynamic environments. However, they may suffer from issues like chattering, sensitivity to model accuracy, or complexity in controller design. Intelligent control strategies, such as those based on Reinforcement Learning (RL), deep learning, or fuzzy logic, have recently gained attention for their ability to handle uncertain and dynamic systems. Nevertheless, these methods frequently require extensive training data, and their performance may degrade in unseen scenarios or lack formal stability guarantees.

Despite these advances, many existing methods struggle to achieve a balanced trade-off between robustness and adaptability in uncertain and cluttered environments. Moreover, several approaches assume full-state feedback or centralized access to the absolute positions of all swarm agents to maintain formation and coordination, which increases complexity and limits scalability. In contrast, the strategy proposed in this paper requires only the leader's (target's) position, without the need for each agent to know the exact state of the others. This significantly simplifies the formation control algorithm, reduces reliance on global information, and enhances the practicality and scalability of swarm coordination. To overcome these limitations, this study proposes a hybrid cooperative control strategy combining a backstepping controller with a formation control law.

The backstepping approach is responsible for ensuring the stability and trajectory tracking of each individual UAV, while the formation controller maintains the desired geometric configuration of the swarm around a moving target. Backstepping was chosen due to its recursive design structure and its ability to guarantee system stability through Lyapunov-based construction, particularly for nonlinear dynamics. Furthermore, an optimization layer is integrated to adaptively tune the control gains, improving overall performance and reducing the need for manual tuning. The main contribution of this paper lies in the development of a cooperative formation control strategy for quadrotor swarms with an optimized backstepping controller that ensures stable and coordinated motion. The proposed approach adopts a decentralized control architecture, where each drone independently computes and tracks its desired trajectory based only on the leader's (target's) motion, without requiring inter-agent communication or knowledge of neighbors states. While formation coordination relies solely on

leader-based information, collision avoidance remains local, enabling each UAV to independently detect and avoid obstacles using its own sensing or predefined rules. This hybrid structure reduces communication overhead and computational load compared to fully decentralized strategies, while ensuring global coordination. Specifically tailored to maintain a pentagonal formation, the method demonstrates precise trajectory tracking, robust disturbance rejection, and effective preservation of inter-agent spacing. These advantages highlight the practicality and scalability of the proposed solution for real-world multi-UAV missions in communication-limited environments.

The remainder of the paper is structured as follows: Section 2 provides a comprehensive description of the nonlinear dynamic model of the quadrotor, including the effects of external wind disturbances. In Section 3, the design methodology of the Backstepping controller is detailed, followed by the application of the Flower Pollination Algorithm to optimize its gains and enhance control performance. Section 4 introduces the formation control strategy, integrated with a collision-avoidance mechanism. Finally, Section 5 presents and analyzes the simulation results that validate the effectiveness and robustness of the proposed control approach under realist wind profile followed by a comparison with other works in the literature.

2. Quadcopter Modelling

A quadcopter is a four-rotor drone that flies and maneuvers by adjusting the speed of its propellers. It is a 6-degree-of-freedom (6DOF) system: 3 linear movements on the x, y and z axes with 3 angular movements (roll ϕ, pitch θ and yaw ψ) around the same 3 axes successively (Fig. 1).

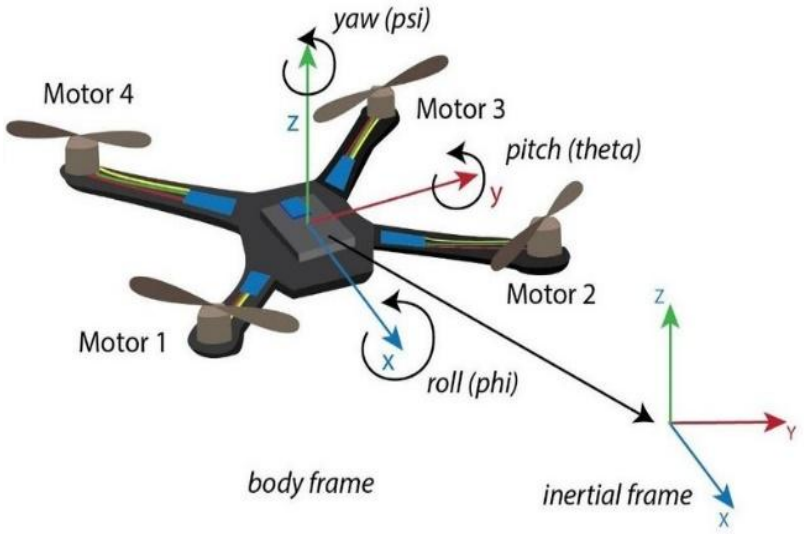

Fig. 1. Quadcopter 6-DOF

The quadcopter is a nonlinear under-actuated system with an input vector of 4 control signals $[U_1 \quad U_2 \quad U_3 \quad U_4]$ and an output vector of 6 variables $[\phi \quad \theta \quad \psi \quad x \quad y \quad z]$. The following assumptions are considered in order to simplify the modeling process and to establish a structured nonlinear state-space representation of the quadrotor system:

The quadrotor is considered as a rigid body with symmetrical structure and evenly distributed mass. The aerodynamic drag forces are modeled along each translational axis using the coefficients $[K_x \quad K_y \quad K_z]$ and are proportional to the corresponding linear velocities. Wind disturbances are included in the dynamic model as external force components $[F_x^w \quad F_y^w]$. The inertial coupling between roll, pitch, and yaw is considered through the full dynamic equations without simplification. The motor dynamics and delays are not modeled explicitly and are assumed to be instantaneous. The modeling retains all gyroscopic coupling terms, thereby fully accounting for inertial interactions between roll ϕ, pitch θ, and yaw ψ dynamics.

$$\begin{cases} \dot{x}_1 = x_2 \\ \dot{x}_2 = \dfrac{I_y - I_z}{I_x} x_4 x_6 + \dfrac{L}{I_x} U_2 \\ \dot{x}_3 = x_4 \\ \dot{x}_4 = \dfrac{I_z - I_x}{I_y} x_2 x_6 + \dfrac{L}{I_y} U_3 \\ \dot{x}_5 = x_6 \\ \dot{x}_6 = \dfrac{I_x - I_y}{I_z} x_2 x_4 + \dfrac{L}{I_z} U_4 \\ \dot{x}_7 = x_8 \\ \dot{x}_8 = \dfrac{cosx_1.sinx_3.cosx_5 + sinx_1.sinx_5}{m} U_1 - \dfrac{K_x x_8}{m} + \dfrac{1}{I_x} F_x^w \\ \dot{x}_9 = x_{10} \\ \dot{x}_{10} = \dfrac{cosx_1.sinx_3.sin - sinx_1.cosx_5}{m} U_1 - \dfrac{K_y x_{10}}{m} + \dfrac{1}{I_y} F_y^w \\ \dot{x}_{11} = x_{12} \\ \dot{x}_{12} = \dfrac{cosx_1.cosx_3}{m} U_1 - \dfrac{K_z x_{12}}{m} - g \end{cases} \quad (1)$$

Where state variables are angular positions and velocities with linear positions and velocities are: $[x_1 \quad x_2 \quad x_3 \quad x_4 \quad x_5 \quad x_6 \quad x_7 \quad x_8 \quad x_9 \quad x_{10} \quad x_{11} \quad x_{12}] = [\phi \quad \dot{\phi} \quad \theta \quad \dot{\theta} \quad \psi \quad \dot{\psi} \quad x \quad \dot{x} \quad y \quad \dot{y} \quad z \quad \dot{z}]$

Simulation parameters are presented in Table 1.

Table 1. Simulation parameters

Parameter	Symbol	Value
Inertia on x axis	I_x	0.0038
Inertia on y axis	I_y	0.0038
Inertia on z axis	I_z	0.0071
Gravitational constant	g	9.81 Kg/s^2
Mass of quadcopter	m	0.486 Kg
Distance between quadcopter's center and each rotor	L	0.25 m
Aerodynamic drag coefficient for x axis motion	K_x	0.0056
Aerodynamic drag coefficient for y axis motion	K_y	0.0056
Aerodynamic drag coefficient for z axis motion	K_z	0.0064

Backstepping control is a nonlinear control technique used to stabilize systems with known or partially known dynamics. It's particularly useful for controlling complex systems like quadcopters, which have highly nonlinear dynamics and are subject to various external disturbances. In Backstepping control, the idea is to design a series of feedback controllers, each of which is responsible for stabilizing a specific state of the system. In this study, Backstepping is applied to stabilize position (x,y, z) and orientation angle (ψ) of the quadcopter (Fig. 2).

3. Optimized Backstepping Control of Quadcopter

3.1. Backstepping Control

Taking the subsystem of angular roll displacement ϕ which is the first state variable x_1 in the overall quadcopter state space model presented in equation's system (2).

$$\dot{x}_1 = x_2 \quad (2)$$

$$\dot{x}_2 = \frac{I_y - I_z}{I_x} x_4 x_6 + \frac{L}{I_x} U_2 \tag{3}$$

- **Step 1**:

Position roll angle error e_1 is:

$$e_1 = x_{1d} - x_1 \tag{4}$$

Selecting a Lyapunov function for e_1 entails ensuring its positivity while its derivative remains negative semi-definite so the error e_1 converges to 0. Lyapunov function is chosen as follows:

$$f(e_1) = \frac{1}{2} {e_1}^2 \tag{5}$$

The derivative of $f(e_1)$is:

$$\dot{f}(e_1) = e_1 \dot{e}_1 = e_1(\dot{x}_{1d} - \dot{x}_1) \tag{6}$$

Then $\dot{x}_1$is replaced by x_2 :

$$\dot{f}(e_1) = e_1(\dot{x}_{1d} - x_2) \tag{7}$$

Variable state $x_2$must be regulated, to take a value allowing to achieve the condition: $\dot{f}(e_1)$ negative semi definite, which is $x_2 = \dot{x}_{1d} + \alpha_1 e_1$ with a positive gain α_1, so a desired value of x_2 must be tracked:

$$x_{2d} = \dot{x}_{1d} + \alpha_1 e_1 , \quad \alpha_1 > 0 \tag{8}$$

- **Step 2:**

Velocity roll angle error e_2 is:

$$e_2 = x_{2d} - x_2 \tag{9}$$

In this step, Lyapunov function depends on position and velocity errors at the same time:

$$h(e_1, e_2) = \frac{1}{2}({e_1}^2 + {e_2}^2) \tag{10}$$

Derivative of the second Lyapunov function is:

$$h(e_1, e_2) = e_1 \dot{e}_1 + e_2 \dot{e}_2 \tag{11}$$

By replacing x_{2d} in equation (9) as it mentioned in the equation (8), equation (12) is obtained:

$$e_2 = \dot{x}_{1d} + \alpha_1 e_1 - x_2 \tag{12}$$

So:

$$e_2 = \dot{e}_1 + \alpha_1 e_1 \tag{13}$$

Error $\dot{e}_1$ is calculated from equation (13):

$$\dot{e}_1 = e_2 - \alpha_1 e_1 \tag{14}$$

Equation (12) is derived to obtain $\dot{e}_2$:

$$\dot{e}_2 = \ddot{x}_{1d} + \alpha_1 \dot{e}_1 - \dot{x}_2 \tag{15}$$

The derivative of second Lyapunov function is:

$$\dot{h}(e_1, e_2) = e_1(e_2 - \alpha_1 e_1) + e_2(\ddot{x}_{1d} + \alpha_1 \dot{e}_1 - \dot{x}_2) \tag{16}$$

$\dot{x}_2$ is replaced by $\frac{I_y - I_z}{I_x} x_4 x_6 + \frac{L}{I_x} U_2$ using equation (2), and by applying Lyapunov theory, control input signal U_2 can be concluded from the equation (16), as:

$$U_2 = \frac{I_x}{L}(\ddot{x}_{1d} + e_1 + \alpha_1 e_2 - {\alpha_1}^2 e_1 - \frac{I_y - I_z}{I_x} x_4 x_6 + \alpha_2 e_2) \tag{17}$$

Such as: $\alpha_1 > 0, \alpha_2 > 0$

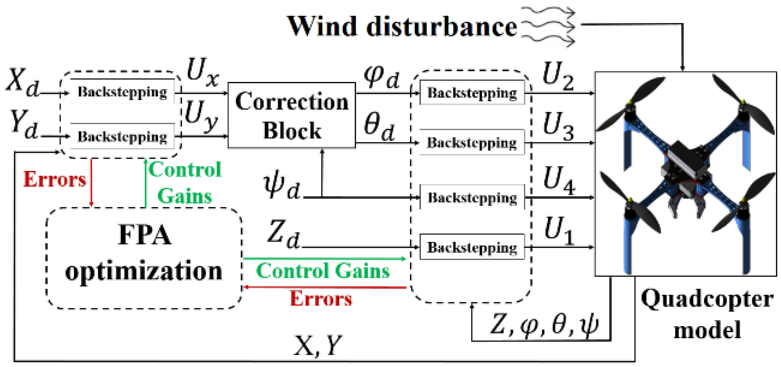

Fig. 2. Controller structure

This is the control law of the 1st state variable φ and control laws of the other degrees of freedom, θ and ψ are obtained by applying Backstepping control in the same way:

$$U_1 = \frac{m}{\cos x_1 \cos x_3}(e_{11} + \ddot{x}_{11d} + \alpha_{11} e_{12} - {\alpha_{11}}^2 e_{11} + g + \frac{k_z x_{12}}{m} + \alpha_{12} e_{12}) \tag{18}$$

$$U_3 = \frac{I_y}{L}(\ddot{x}_{3d} + e_3 + \alpha_3 e_4 - {\alpha_3}^2 e_3 - \frac{I_z - I_x}{I_y} x_2 x_6 + \alpha_4 e_4) \tag{19}$$

$$U_4 = \frac{I_z}{L}(\ddot{x}_{5d} + e_5 + \alpha_5 e_6 - {\alpha_5}^2 e_5 - \frac{I_x - I_y}{I_z} x_4 x_2 + \alpha_6 e_6) \tag{20}$$

Where: $\alpha_s > 0 \quad , \quad \forall\, s$

Because the quadcopter is an under actuated system, a virtual control input U_x and U_y must be developed to make a position control, by calculating the appropriate roll ϕ_d and pitch θ_d angles, which ensure the desired x and y positions, represented by the correction block in Fig. 2.

$$x_{1d} = \sin^{-1}(U_x \sin x_{5d} - U_y \cos x_{5d}) \tag{21}$$

$$x_{3d} = \sin^{-1}\left(\frac{U_x \cos x_{5d} + U_y \sin x_{5d}}{\cos x_{1d}}\right) \tag{22}$$

By applying Backstepping control on the x and y position subsystems (x_7 and x_9 state variables successively) mentioned in the overall quadcopter system (Equation (2)), virtual control input U_x and U_y are found in the same way as other control input signals.

$$U_x = \frac{m}{U_1}(e_7 + \ddot{x}_{7d} + \alpha_7 e_8 - {\alpha_7}^2 e_7 + \frac{k_x x_8}{m} + \alpha_8 e_8 - \frac{1}{I_x} F_x^w) \tag{23}$$

$$U_y = \frac{m}{U_1}(e_9 + \ddot{x}_{9d} + \alpha_9 e_{10} - {\alpha_9}^2 e_9 + \frac{k_y x_{10}}{m} + \alpha_{10} e_{10} - \frac{1}{I_y} F_y^w) \tag{24}$$

Where: $\alpha_s > 0 \quad , \quad \forall s$

3.2. FPA Optimization

The Flower Pollination Algorithm FPA (Fig. 3) is a metaheuristic optimization method used to tune the gains of a previously designed Backstepping controller by minimizing the Integral Squared Error (ISE) over the simulation time t_{sim}, aiming to enhance system performance [60].

$$ISE = \int_0^{t_{sim}} 3e_x^2(t) + 3e_y^2(t) + e_z^2(t) + 2e_\phi^2(t) + 2e_\theta^2(t) + e_\psi^2(t)\, dt \quad (25)$$

Initialize: Number of iteration $iter$, Population size N, Switching probability p, step size c

Evaluate initial population and find the best solution $gbest$

For $i = 1 \rightarrow iter$

For $j = 1 \rightarrow N$

If $rand < p$

Do $x_i^{t+1} = x_i^t + rand.c(x_i^t - gbest$ **(Global pollination)**

Else

Select 2 random solutions x_m^t and x_n^t

Do $x_i^{t+1} = x_i^t + rand.(x_m^t - x_n^t)$ **(Local pollination)**

End if

Select and update solution

End for

Find the current best solution among the population

End for

Extract the optimal solution x (Optimal Backstepping gains)

$$x_i = [\alpha_1(i)\alpha_2(i)\alpha_3(i)\alpha_4(i)\alpha_5(i)\alpha_6(i)$$
$$\alpha_7(i)\alpha_8(i)\alpha_9(i)\alpha_{10}(i)\ \alpha_{11}(i)\ \alpha_{12}(i)]$$

Fig. 3. Applied flower pollination algorithm [60]

Table 2 presents the best FPA's parameters used in simulation after many tests.

Table 2. FPA parameters

Parameter	Symbol	Value
Number of variables (Backstepping gains)	var	12
Search range	$[a \ \ b]$	[0 12]
Population	N	50
Number of Iteration	$iter$	14
Switching probability	p	0.04
Step size	c	0.02

The Flower Pollination Algorithm (FPA) is adopted for its simplicity, requiring few parameters to adjust, and for its fast convergence within only a few iterations compared to other metaheuristics such as PSO and ACO [60]. The strong performance achieved by the FPA-optimized backstepping controller shows that this offline optimization approach can provide highly effective and well-tuned gains.

4. Formation Control

Quadcopters swarm of this application is a multi-UAV system composed of 6 quadcopters (Leader and 5 followers) as it is presented in Fig. 4 (a), the Leader UAV_L is controlled by Backstepping optimized in FPA explained previously to follow a predefined trajectory and the five quadcopter followers (from UAV_{F1} to UAV_{F5}) are controlled each one by the same technique to follow different trajectories received from the proposed formation controller to compose a desired formation and tracking this Leader.

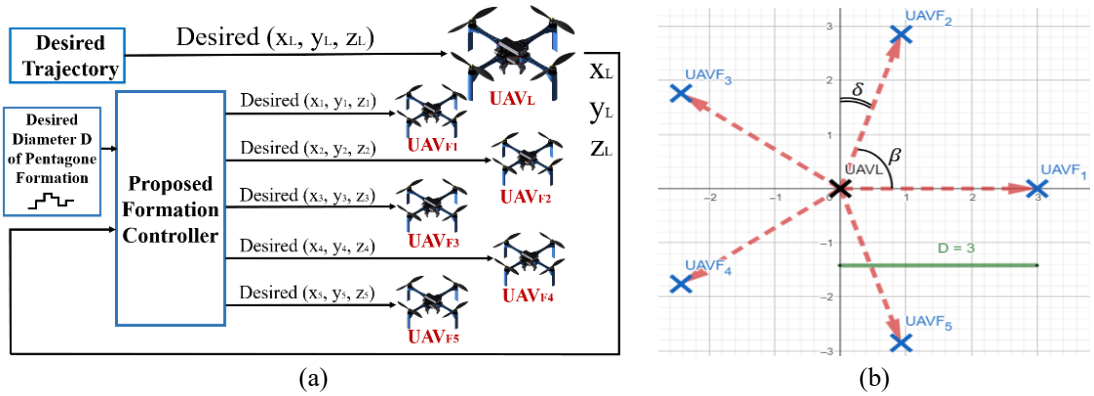

(a) (b)

Fig. 4. (a) Proposed formation control strategy (b) Pentagonal formation used by formation controller

The role of formation controller is to generate the suitable trajectory for each UAV_{Fi} from the current position of the leader UAV_L (Feedback) and the diameter D of the desired shape (set point) presented in Fig. 4 (b). Each follower UAV_{Fi} receives a desired trajectory (x_{dFi}, x_{dFi}) as dynamic coordinates in the (x , y) plane generated to compose the pentagon shape which must be kept during the entire time of the Leader's movement (Fig. 4 (a)). In the case of a change in the positioning order of the UAV followers during leader tracking or in the first seconds, where each drone positions itself at the location requested by the formation controller. A collision between two drones may occur, so an algorithm is proposed to prevent this problem. The algorithm adjusts the altitude z of the UAV followers, allowing them to ascend or descend while maintaining their position in the (x , y) plane (Fig. 5).

Intialisation
Test time: $t_{final} = 180\ s$ *UAVs Followers number*: $N = 5$
Pentagone Diameter: $D = 1\ m$
Altitude of swarm: $z = 2\ m$
Positions of UAVs Followers :
for $i = 1 \rightarrow N$:
(UAV_{Fi}) *coordinates* $= (x_i, y_i, z_i)$
end
Position of UAV Leader : (UAV_L) *coordinates* $= (x_L, y_L, z_L)$ /
Distance of security : $\tilde{D} = 0.8\ m$ / *Anti collision altitude* : $\check{Z} = 0.4\ m$
Begin
for $t = 0 \rightarrow t_{final}$
for $i = 1 \rightarrow N$
$z_i = z_L$
end

$\{x_1 = x_L + D; y_1 = y_L\}$
$\{x_2 = x_L + D.\sin(\delta); y_2 = y_L + D.\cos(\alpha)\}$
$\{x_3 = x_L - D.\sin(\delta); y_3 = y_L + D.\cos(\delta)\}$
$\{x_4 = x_L - D.\sin(\delta); y_4 = y_L - D.\cos(\delta)\}$
$\{x_5 = x_L + D.\sin(\alpha); y_5 = y_L - D.\cos(\alpha)\}$
for $i = 1 \rightarrow N$
for $j = 1 \rightarrow N$; $j \neq i$
$d = \sqrt{(x_i - x_j)^2 + (y_i - y_j)^2}$
if $d \leq \tilde{D}$:
$z_i = z_L \mp \check{Z}$
else
$z_i = z_L$
end
end
end
End

Fig. 5. Formation controller algorithm with anti-collision technique

The proposed algorithm presents a good idea to maintain the desired shape in the plane (x, y), and avoid the collision at the same time by checking the distance between UAV_{Fi} and UAV_{Fj}.To avoid the collision, a safety distance is determined by taking into consideration the length between the center of the drone and each motor which is $0.25\ m$, then the collision is made effectively when the distance between two drones is $\leq 0.5\ m$, this is why the safety distance is $\tilde{D} = 0.8\ m$ to move away from the collision. In the case where the distance between two follower drones is less than the safety distance

$\tilde{D}$, one of the UAV_{Fi} changes the altitude by $0.4\ m$ while keeping the position, which maintains the pentagon shape in the horizontal plane (x, y).The proposed methodology is summarized starting from the individual control of each swarm agent (drone), moving through the applied metaheuristic optimization, and culminating in the formation control strategy designed to maintain a pentagon-shaped configuration (Fig. 6).

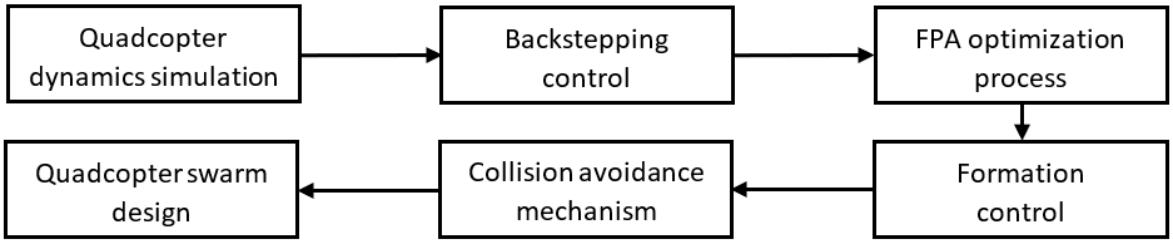

Fig. 6. Flowchart of the proposed methodology for swarm formation control

The proposed method relies first on an individual backstepping controller for each drone in the swarm to ensure independent trajectory tracking (Fig. 2). Then, a formation controller computes the appropriate desired trajectory for each agent (drone) so that all drones maintain a pentagonal formation, with the center of the pentagon following the global target (leader) along any arbitrary trajectory (Fig. 4). Additionally, the system is equipped with a collision avoidance mechanism based on altitude adjustment when necessary (Fig. 5).

5. Results and Discussion

The optimization procedure by the FPA algorithm is applied according to the optimization parameters in Table 2 to minimize the objective function: Integral Squared Error (ISE).

Table 3 summarizes the convergence performance of the Flower Pollination Algorithm (FPA) in terms of Integral Squared Error (ISE) reduction across 14 optimization iterations. It can be observed that in all tested runs, the ISE decreased noticeably from its initial value to the final optimized value, with improvement rates ranging from 10.67% to 35.45%. This consistent reduction clearly demonstrates the effectiveness of the FPA in enhancing controller performance. On average, the improvement exceeded 21%, confirming the robustness of the optimization process. Furthermore, the optimization converged within a limited number of iterations, ensuring a satisfactory trade-off between accuracy and computational effort. These findings highlight the capability of the proposed approach to achieve reliable convergence while minimizing control error.

Table 4 presents backstepping control gains. This section presents and analyzes the key results obtained from the implementation of the proposed control strategy. First, the quadcopter's trajectory tracking performance is evaluated. Then, the results of target (Leader) tracking by the drone swarm are discussed, based on three different trajectory scenarios designed to validate the flexibility and adaptability of the proposed method. Subsequently, robustness tests and collision avoidance capabilities are analyzed. Finally, a comparative discussion with previous studies is provided, followed by a summary of the strengths and limitations of the proposed approach.

5.1. Quadcopter Backstepping Control

To evaluate the performance of the designed controller, this section analyzes the quadcopter's step responses and trajectory tracking results, while taking into account the imposed constraints on roll and pitch angle limits, as well as control input saturation.

5.1.1. Step Response

The step responses of quadcopter to desired position x_d, y_d, altitude z_d and orientation ϕ_d are tested for this set-points: $[x_d = 1m \quad y_d = 1m \quad z_d = 1m \quad \psi_d = 25°]$. Fig. 7 (a) presents the quadcopter responses to a step of (x, y) positions and z altitude. The results show good performances,

with different settling times: For $(x, y) = 1.5s$, for $z = 1s$ and for $\psi < 1s$. All responses are without overshoot or steady-state error which shows the good stability and precision of designed controller. According to Fig. 7 (b), roll and pitch angles reaches $[-45° \quad 45°]$ as a maximum range to make quadcopter going to desired (x, y) positions, so they do not exceed the limit $\left[-\frac{\pi}{2} \quad \frac{\pi}{2}\right]$ mentioned previously with the mathematical model of quadcopter.

Table 3. ISE improvement achieved by FPA optimization over 14 iterations

Run	Initial ISE	Final ISE	Improvement (%)
1	59.24	52.92	10.67%
2	60.47	51.84	14.27%
3	60.34	45.15	25.17%
5	68.35	44.12	35.45%

Table 4. Obtained control gains

State variable	1st gain	2nd gain
Roll angle ϕ	$\alpha_1 = 4.4025$	$\alpha_2 = 9.3048$
Pitch angle θ	$\alpha_3 = 6.4184$	$\alpha_4 = 5.0494$
Yaw angle ψ	$\alpha_5 = 7.6955$	$\alpha_6 = 2.2141$
Position x	$\alpha_7 = 4.8548$	$\alpha_8 = 7.0579$
Position y	$\alpha_9 = 4.4025$	$\alpha_{10} = 6.6385$
Altitude z	$\alpha_{11} = 6.1893$	$\alpha_{12} = 3.5344$

Where: F_1 , F_2 , F_3 and F_4 are the thrust forces of the four motors of the quadcopter. The force values demanded by the controller are both reasonable and achievable (Fig. 8), as they remain within the typical operational limits of commonly used drone motors (i.e., brushless motors). The effectiveness of the proposed controller is further demonstrated by its ability to respect the imposed constraints on roll and pitch angles, as well as on the control input signals.

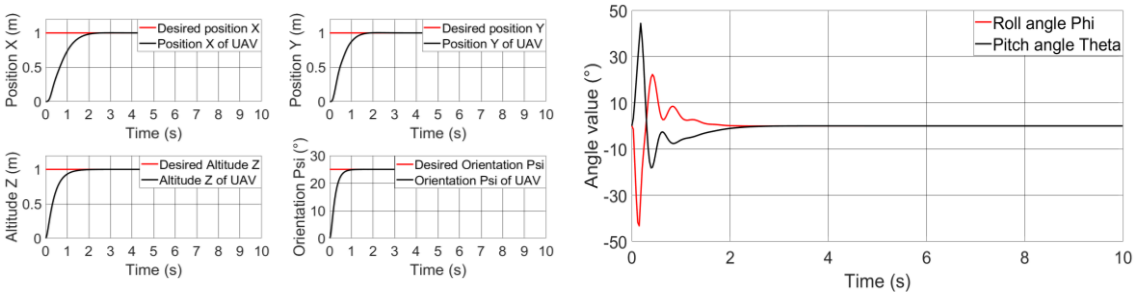

(a) (b)

Fig. 7. (a) Step response of x, y, z and ψ (b) Roll ϕ and pitch θ corresponding responses

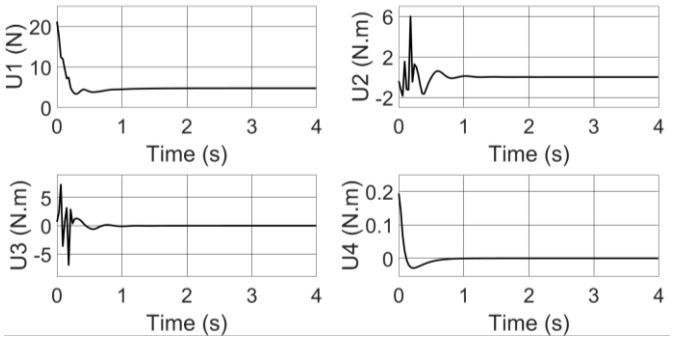

Fig. 8. Control input signals

$[U_1 \quad U_2 \quad U_3 \quad U_4]$ are the control inputs of the quadcopter described mathematically as follows:

$$U_1 = F_1 + F_2 + F_3 + F_4 \tag{26}$$

$$U_2 = F_3 - F_1 \tag{27}$$

$$U_3 = F_4 - F_2 \tag{28}$$

$$U_4 = F_1 - F_2 + F_3 - F_4 \tag{29}$$

5.1.2. Trajectory Tracking

Desired trajectory is developed by desired positions x, y and z signals as follows:

$$\begin{cases} x_d = 2.5\sin(0.08t) \\ y_d = 2.5\sin(0.04t) \\ z_d = 2 \end{cases} \tag{30}$$

According to results presented in Fig. 9 (a), quadcopter tracks sinusoidal trajectory with a high precision, where the error between desired and real positions is 10^{-2}(almost zero). Fig. 9 (b) illustrates the 3D motion of the quadcopter during the execution of the lemniscate trajectory (∞), following the appropriate reference signals (desired x, y and z) depicted in Fig. 9 (a), while maintaining a constant altitude of 2 meters. The results clearly demonstrate that the quadcopter is capable of accurately tracking the desired trajectory with high stability and precision, confirming the robustness and effectiveness of the proposed control strategy.

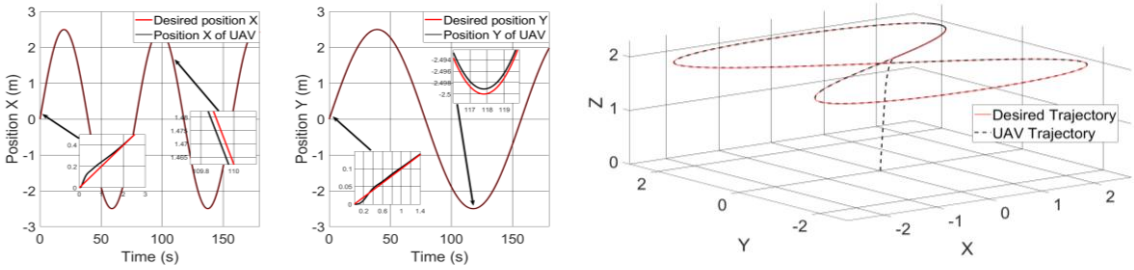

(a) (b)

Fig. 9. (a) x and y positions response to a sinusoidal reference (b) Corresponding 3D presentation of quadcopter trajectory tracking

5.2. Leader Tracking by Quadcopters Swarm

The drone leader UAV_L is the drone to follow, for a surveillance objective by drones UAV_{Fi} and the following simulation result shows the accuracy of Pentagon formation control. Different scenarios are simulated to present the formation flying tests under the control of the proposed strategy. Each scenario has different initial positions of the drones and different trajectories to follow, it is detailed in 4 steps presented in 2 and 3 dimensions and the result of Fig. 10 is obtained by simulating the first scenario. Motion of overall swarm is presented based on different scenarios of flying tracking in the following figures to show the simulation tests of the proposed formation controller.

5.2.1. First Scenario

Initial position in meter of each UAV is:

$$\begin{cases} UAV_L: x_i = 0\ ;\ y_i = 0 \\ UAV_{F1}: x_i = 1.5\ ;\ y_i = 0 \\ UAV_{F2}: x_i = 3\ ;\ y_i = 0 \\ UAV_{F3}: x_i = -1.5\ ;\ y_i = 0 \\ UAV_{F4}: x_i = -3\ ;\ y_i = 0 \\ UAV_{F5}: x_i = 0\ ;\ y_i = -1.5 \end{cases} \tag{31}$$

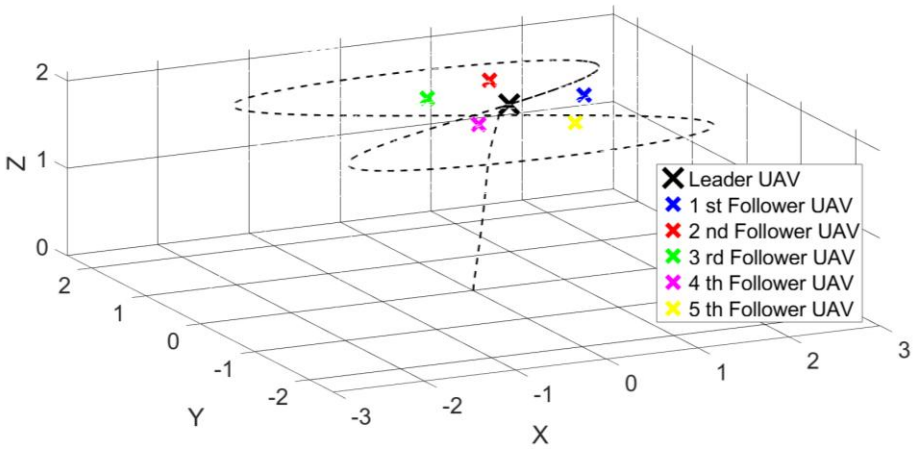

Fig. 10. Leader tracking by quadcopters swarm in 3D (in meter)

5.2.2. Second Scenario

Initial position in meter of each UAV is:

$$\begin{cases} UAV_L: x_i = 0.3\ ;\ y_i = 0 \\ UAV_{F1}: x_i = 1.5\ ;\ y_i = 0 \\ UAV_{F2}: x_i = -1.8\ ;\ y_i = 0 \\ UAV_{F3}: x_i = 0\ ;\ y_i = 1.5 \\ UAV_{F4}: x_i = -0.8\ ;\ y_i = -0.6 \\ UAV_{F5}: x_i = 0\ ;\ y_i = -2.7 \end{cases} \quad (32)$$

5.2.3. Third Scenario

Initial position in meter of each UAV is:

$$\begin{cases} UAV_L: x_i = 0\ ;\ y_i = 0 \\ UAV_{F1}: x_i = 1\ ;\ y_i = -1 \\ UAV_{F2}: x_i = 1\ ;\ y_i = 2 \\ UAV_{F3}: x_i = -1\ ;\ y_i = -1 \\ UAV_{F4}: x_i = -2\ ;\ y_i = -2 \\ UAV_{F5}: x_i = -2\ ;\ y_i = 2 \end{cases} \quad (33)$$

In all scenarios (Fig. 11, Fig. 12 and Fig. 13), the 4 steps of swarm movement are explained as follows:

- Step 1 shows the drones on their initial positions.
- Step 2 presents the start-up of the drone leader UAV_L to follow its desired trajectory and the start-up of the drones UAV_{Fi} for the leader tracking.
- Step 3: Pentagon formation is composed quickly with the desired D and the tracking of the leader is beginning.
- Step 4: Drones UAV_{Fi} keep the pentagon formation while following the leader.

Followers UAV_{Fi} apply a good and continuous tracking the UAV_L, which shows the stability and precision of the proposed formation controller. To check the operation of the swarm in the event of a change in the diameter of the Pentagon formation, another test of 30 seconds is simulated using a desired variable diameter as follows:

$$\begin{cases} D = 1m \quad for: \quad 0s \le t < 6s \\ D = 1.7m \quad for: \quad 6s \le t < 11s \\ D = 1.2m \quad for: \quad 11s \le t < 16s \\ D = 2m \quad for: \quad t \ge 16s \end{cases} \quad (34)$$

Fig. 14 show the stability and precision of controller in pentagon formation tracking by the swarm with a variable diameter of pentagon shape and also shows the rapidity of providing the desired formation with a settling time of $\approx 3s$.

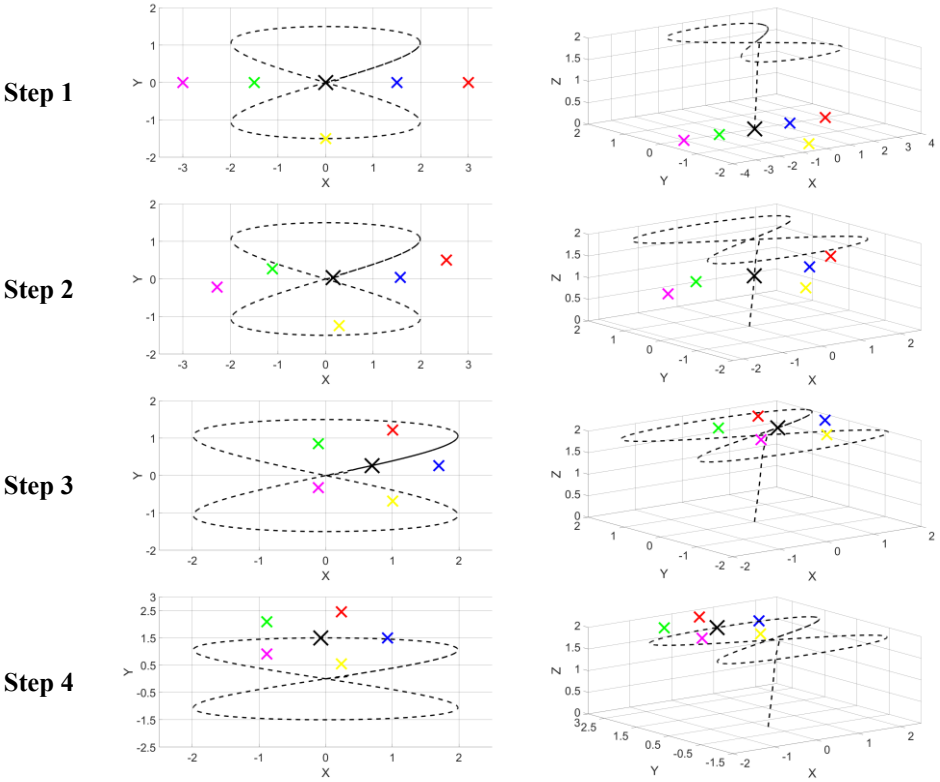

Fig. 11. Lemniscate trajectory (∞) tracking by the swarm

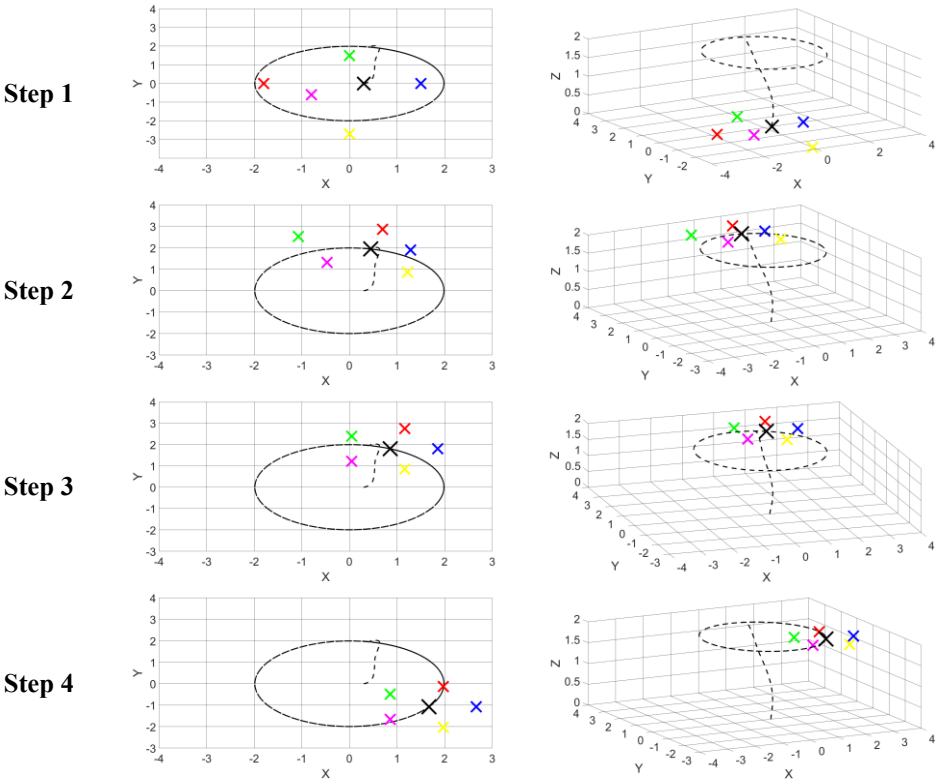

Fig. 12. Circular trajectory tracking by the swarm

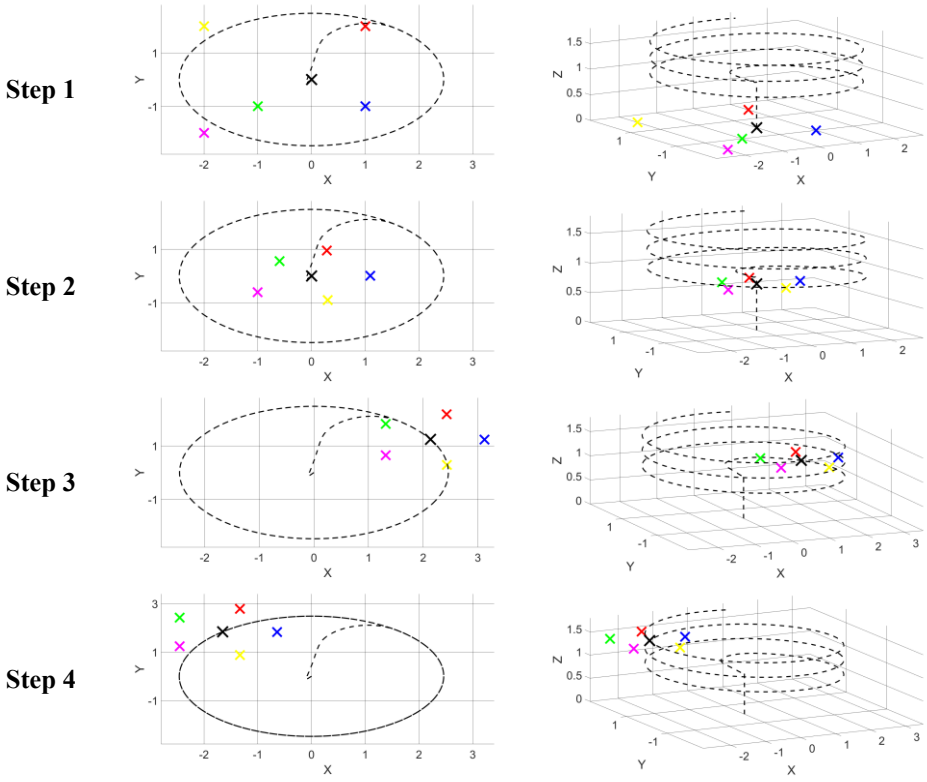

Fig. 13. Ascending orbit trajectory tracking by the swarm

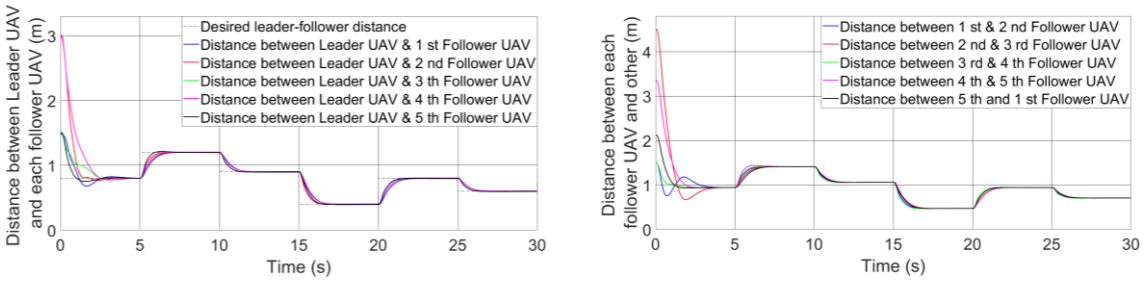

Fig. 14. Distance between the leader UAV_L and each follower UAV_{Fi} (Left figure) Distance between followers drones UAV_{Fi} (Right figure)

5.3. Robustness and Anti-Collision

To evaluate the robustness of the developed backstepping controller, external wind disturbances were introduced at various time intervals. The disturbance F_x^w is applied during the interval [20s - 50s], followed by a combination of F_x^w and F_y^w during [50s - 180s]. A realistic wind profile is applied as a disturbance to test the robustness of the quadrotor control system. The wind velocities V_x and V_y along the x- and y-axes is modeled as the sum of a steady mean component and a time-correlated turbulent component, characterized by specific correlation time and turbulence intensity parameters. The resulting wind velocity equations for each axis are as follows:

$$V_x(t) = [5.2 + 2sin(0.05t) + 0.5sin(0.5t)] + X_x(t)$$
$$V_y(t) = [3 + 1.5sin(0.04t + \pi/3)] + X_y(t) \quad (35)$$

Here, $X_x(t)$ and $X_y(t)$ represent the turbulent variations over time:

$$X_x(t) = \alpha_x X_x(t - \Delta t) + \sigma_x \sqrt{1 - {\alpha_x}^2}\eta_x(t), \alpha_x = e^{\frac{-\Delta t}{\tau_x}} \quad (36)$$

$$X_y(t) = \alpha_y X_y(t - \Delta t) + \sigma_y \sqrt{1 - {\alpha_y}^2}\eta_y(t)\,, \alpha_y = e^{\frac{-\Delta t}{\tau_y}}$$

Where: τ is the correlation time (s), σ is the turbulence intensity (m/s), and η is a Gaussian white noise process. The wind disturbance acting on the quadrotor is modeled using the classical aerodynamic drag formulation:

$$F_x^w = \frac{1}{2}\sigma C_d A {V_x}^2 \quad , \quad F_y^w = \frac{1}{2}\sigma C_d A {V_y}^2 \tag{37}$$

Where $\rho = 1.225\ kg/m^3$ is the air density at sea level under standard atmospheric conditions, $Cd = 1$ is a typical drag coefficient for small quadrotors with blunt geometries, $A = 0.025\ m^2$ represents the estimated frontal area of the $0.5\ kg$ quadrotor, and V is the wind speed. The values of Cd and A are consistent with common geometrical and aerodynamic characteristics reported for small multi-rotor UAVs in low-speed regimes [61]. The Fig. 15 illustrates the position tracking performance of the quadrotor under these varying conditions. It includes six plots: the position responses along x and y axis and the corresponding disturbance signals $[F_x^w \quad F_y^w]$.

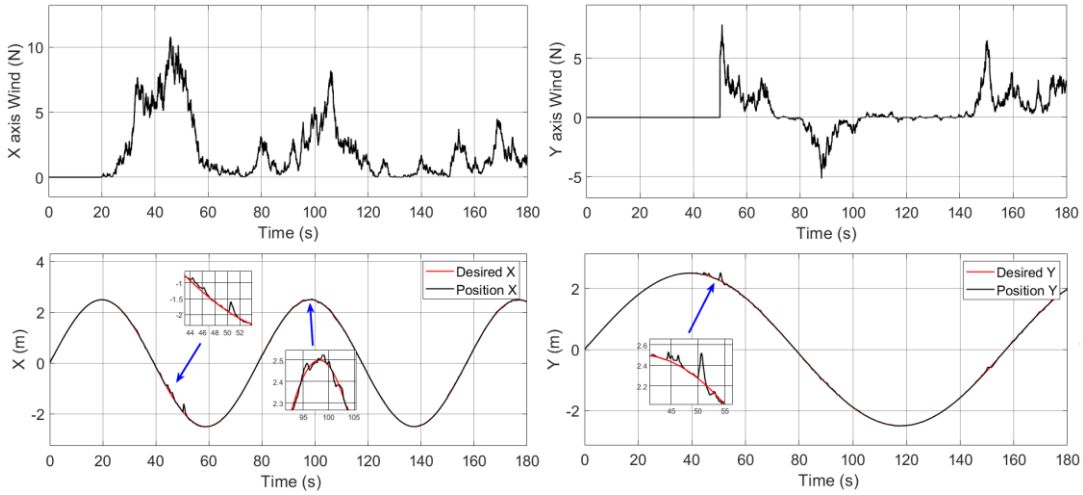

Fig. 15. Trajectory tracking under wind disturbance by one drone

The quadrotor accurately follows the desired trajectory during the initial phase. When the realistic turbulent wind disturbance force F_x^w is applied between 20 s and 50 s, a noticeable but limited deviation appears along the x-direction. This wind profile, based on realistic turbulence characteristics, contains both low-frequency and high-frequency components. From 50 s to 180 s, the additional lateral disturbance F_y^w is introduced, also following the realistic turbulent wind profile. The simultaneous presence of disturbances in both the x and y directions is particularly challenging, as these axes are dynamically coupled in the quadrotor's mathematical model. Unlike the z-axis, which is controlled separately through thrust and is easier to stabilize, controlling x and y positions is more complex and sensitive to external influences. Despite these sustained turbulent disturbances, the quadrotor remains stable, and the trajectory tracking errors do not diverge. The brief deviations observed when the wind forces are applied are quickly corrected, confirming the robustness and effectiveness of the developed backstepping controller in maintaining accurate tracking performance under realistic wind disturbances (Fig. 15). Table 5 presents the RMSE values computed using equation (38), for the two circular trajectory and Lemniscate (∞) scenarios obtained by a 180 s test, both without and with wind disturbance.

$$RMSE_i = \sqrt{\frac{1}{k}\sum_{t=1}^{k} {e_i}^2} \quad , \quad \forall\, i \in \{x, y, \phi, \theta\} \quad k = \frac{180}{T} \tag{38}$$

Where: $T = 0.01$ is the simulation sampling time. The wind profile applied corresponds to the robustness test illustrated in Fig. 15. The considered errors are those of positions (x, y) and angles (roll/pitch) since these four degrees of freedom are the most critical ones affecting the preservation of the desired pentagonal formation of the swarm.

Table 5. RMSE with and without wind disturbance

Studied Case		Root Mean Square Error *RMSE*			
		Position x (m)	**Position y (m)**	**Roll angle ϕ (°)**	**Pitch angle θ (°)**
Circular trajectory	Without wind disturbance	0.0156	0.0631	0.0397	0.0688
	Under wind disturbance	0.0398	0.0689	0.1205	0.1965
Lemniscate trajectory (∞)	Without wind disturbance	0.0075	0.0041	0.0173	0.0379
	Under wind disturbance	0.0321	0.0249	0.1125	0.1841

The 3D trajectory plot illustrates the quadrotor's ability to accurately follow the desired path in three-dimensional space. When wind disturbances are introduced, the quadrotor exhibits slight deviations from the reference trajectory. However, these deviations remain limited and do not lead to instability or error divergence. The trajectory remains smooth and coherent throughout, confirming the robustness and effectiveness of the proposed backstepping-based control strategy (Fig. 16 (a)).

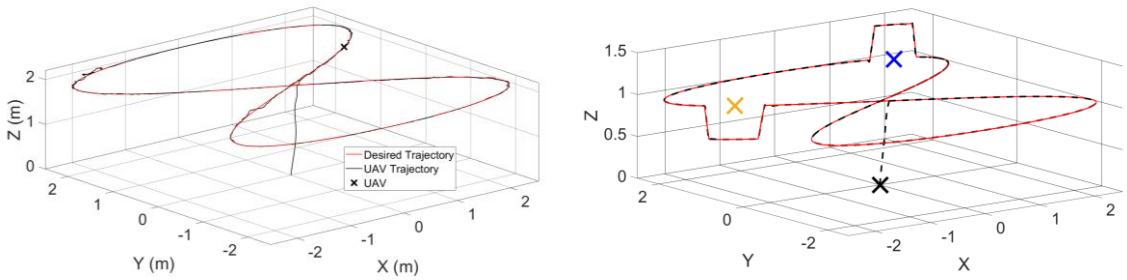

(a) (b)

Fig. 16. (a) Quadrotor trajectory tracking under wind disturbance (b) Anti-collision example

Regarding the security motion system, a scenario of collision is simulated in this part as follows: any drone UAV_{Fi} in the swarm encounters another UAV_{Fj}, where the distance between them is less than the safety distance to test anti-collision, following the proposed algorithm (Fig. 5). Fig. 16 (b) shows the reaction of one drone to avoid collision with two other drones. The black drone UAV_{Fi} changes the altitude by 0.4 meters one upwards to avoid the blue drone and another time downwards to avoid the yellow one, because these two drones enter the security circle of the black UAV during its trajectory tracking. It is clear from this result that a drone UAV_{Fi} can successfully avoid collision with another UAV_{Fj} from the swarm based on the altitude change technique integrated into the overall formation controller algorithm (Fig. 5), without distorting the desired shape on the plane (x, y) (Pentagon).The results presented in this part indicate the robustness and the effectiveness of the proposed drone swarm formation control, which can ensure continuous monitoring of a drone or another flying robot by composing a desired shape.

5.4. Comparison, Strengths and Limitations

Compared with the works reported in the literature, the proposed approach demonstrates several distinctive advantages. Based on the obtained results, the proposed controller stands out with remarkable accuracy, since the steady-state error is zero (steady-state error = 0), unlike several works relying on classical PID controllers where a residual offset remains. Furthermore, the complete absence of overshoot (0%) confirms excellent stability, while other approaches reported in the literature often exhibit significant transient overshoots. In terms of speed, the settling time remains short (between 1 s and 3 s depending on the initial distance of each agent in the formation), placing it among the most efficient methods compared to linear approaches such as LQR, whose effectiveness

strongly depends on the initial conditions. Regarding robustness, simulations show that the backstepping controller maintains its performance even under the influence of a real wind profile, whereas classical PID and LQR controllers experience a significant degradation in accuracy. Unlike sliding mode control (SMC) strategies, the developed scheme does not suffer from any chattering phenomenon, ensuring smooth operation. Finally, the proposed cooperative architecture offers a key advantage in formation: it does not require complex inter-agent communication, unlike consensus-based approaches, where each drone must constantly exchange its position with others to preserve the formation.

The proposed controller does not require each agent to know the positions of others to maintain the pentagonal formation, which significantly reduces communication links and minimizes the impact of delays, losses, or disturbances of communication, nevertheless, some limitations remain (Table 6). The optimization phase can be computationally demanding, and the current framework does not yet handle real-time adaptation to highly dynamic environments. Future work will therefore focus on incorporating adaptive or learning-based extensions to increase flexibility, as well as on developing an integrated analysis of formation stability and safety guarantees for reconfigurable formations.

Table 6. Strengths and limitations

Aspect	Strengths	Limitations and Perspectives
Robustness to disturbances	The proposed method maintains performance under external disturbances	Real-time robustness under high-speed maneuvers or turbulent environments could be further explored.
Cooperative control	Effective decentralized coordination in a multi-agent system, enhancing scalability and autonomy.	Further improvements could focus on enhancing robustness of decentralized cooperation under communication delays.
Trajectory tracking accuracy	Demonstrated high accuracy in both single and multi-agent tracking scenarios.	Performance under GPS-denied environments or partial sensor failure could be further studied.
Anti-collision capability	Integration of potential field ensures safe inter-agent distances in dynamic scenarios.	May require adaptive gain tuning in highly dense environments; an adaptive or AI-based field tuning is envisioned.
Experimental validation	Real-time implementation on quadrotor shows practical applicability.	Validation with more agents and in more complex 3D environments is part of future work.

6. Conclusion

This paper proposed a cooperative formation control strategy for a pentagon-shaped drone swarm tasked with monitoring a target drone. Each quadrotor was guided by a decentralized backstepping controller dedicated to tracking its assigned trajectory, while a formation controller ensured collision avoidance and preserved the desired pentagonal geometry. This two-layered approach allowed stable trajectory tracking at the individual level and safe coordinated motion at the swarm level. The method proved robust against wind disturbances and motor saturation while maintaining accurate tracking and formation stability. Simulations confirmed its effectiveness in terms of stability, accuracy, and robustness, with the pentagon formation preserved without requiring global feedback, thus reducing implementation complexity. In addition to qualitative observations, performance metrics such as overshoot $= 0\%$, settling time $\approx 1.5\ s$, and steady-state accuracy will be reported to provide a more precise quantitative evaluation of the proposed approach.

Compared to existing methods, the proposed strategy offers a balance between simplicity and robustness, ensuring reliable formation maintenance under various initial conditions and trajectories. By accounting for disturbances, actuator limits, and obstacle avoidance within the formation controller, it demonstrates strong practical feasibility for real-world multi-drone applications. Future work will address experimental validation, extension to larger and heterogeneous swarms, and integration of adaptive or learning-based layers to improve robustness in dynamic environments, enabling applications in surveillance, search and rescue, and environmental monitoring.

Author Contribution: All authors contributed equally to the main contributor to this paper. All authors read and approved the final paper.

Funding: This research received no external funding.

Conflicts of Interest: The authors declare no conflict of interest.

References

[1] N. Ahmed and M. Chen, "Robust model reference adaptive backstepping sliding-mode control for quadrotor attitude with disturbance observer," *Aircraft Engineering and Aerospace Technology*, vol. 93, no. 7, pp. 1156-1170, 2021, https://doi.org/10.1108/AEAT-11-2020-0277.

[2] H. Ahn, M. Hu, Y. Chung, and K. You, "Sliding-mode control for flight stability of quadrotor drone using adaptive super-twisting reaching law," *Drones*, vol. 7, no. 8, p. 522, 2023, https://doi.org/10.3390/drones7080522.

[3] M. Karahan, M. Inal, and C. Kasnakoglu, "Fault Tolerant Super Twisting Sliding Mode Control of a Quadrotor UAV Using Control Allocation," *International Journal of Robotics and Control Systems*, vol. 3, no. 2, pp. 270-285, 2023, http://dx.doi.org/10.31763/ijrcs.v3i2.994.

[4] J. Kuang and M. Chen, "Adaptive Sliding Mode Control for Trajectory Tracking of Quadrotor UAV under Input Saturation and Disturbances," *Drones*, vol. 8, no. 11, p. 614, 2024, https://doi.org/10.3390/drones8110614.

[5] M. Lhayani, A. abbou, Y. E. Houm, and H. Mahmoudi, "Adaptive nonsingular fast terminal sliding mode control based finite-time disturbance observer for a quadrotor system," *Proceedings of the Institution of Mechanical Engineers, Part I: Journal of Systems and Control Engineering*, vol. 239, no. 5, pp. 761-789, 2025, https://doi.org/10.1177/09596518241300684.

[6] C. Liang and K. Yang, "Adaptive nonsingular terminal sliding mode tracking control of quadrotor systems with mass uncertainties and input delay," *Transactions of the Institute of Measurement and Control*, vol. 45, no. 15, pp. 3031-3046, 2023, https://doi.org/10.1177/01423312231161140.

[7] M. Maaruf, A. N. Abubakar, and M. M. Gulzar, "Adaptive backstepping and sliding mode control of a quadrotor," *Journal of the Brazilian Society of Mechanical Sciences and Engineering*, vol. 46, no. 11, p. 630, 2024, https://doi.org/10.1007/s40430-024-05188-z.

[8] A. Noordin, M. A. Mohd Basri, and Z. Mohamed, "Adaptive pid control via sliding mode for position tracking of quadrotor mav: Simulation and real-time experiment evaluation," *Aerospace*, vol. 10, no. 6, p. 512, 2023, https://doi.org/10.3390/aerospace10060512.

[9] H. Sang, "Quadrotor UAV Trajectory Tracking Control Based on Adaptive Non-singular Terminal Sliding Mode," *Journal of Electrical Systems*, vol. 20, no. 3, pp. 929-939, 2024, https://doi.org/10.52783/jes.3022.

[10] B. Zheng, Y. Wu, H. Li, and Z. Chen, "Adaptive sliding mode attitude control of quadrotor uavs based on the delta operator framework," *Symmetry*, vol. 14, no. 3, p. 498, 2022, https://doi.org/10.3390/sym14030498.

[11] J. Betancourt, V. Balaguer, P. Castillo, P. García, and R. Lozano, "Robust control scheme based on an uncertainty and disturbance estimator for a quadrotor with motor failures," *Journal of Field Robotics*, vol. 40, no. 5, pp. 1115-1129, 2023, https://doi.org/10.1002/rob.22174.

[12] M. Izadi and R. Faieghi, "High-gain disturbance observer for robust trajectory tracking of quadrotors," *Control Engineering Practice*, vol. 145, p. 105854, 2024, https://doi.org/10.1016/j.conengprac.2024.105854.

[13] S. Mobayen, F. F. El-Sousy, K. A. Alattas, O. Mofid, A. Fekih, and T. Rojsiraphisal, "Adaptive fast-reaching nonsingular terminal sliding mode tracking control for quadrotor UAVs subject to model uncertainties and external disturbances," *Ain Shams Engineering Journal*, vol. 14, no. 8, p. 102059, 2023, https://doi.org/10.1016/j.asej.2022.102059.

[14] J. A. Vazquez Trejo *et al.*, "Robust Formation Control Based on Leader-Following Consensus in Multi-Agent Systems With Faults in the Information Exchange: Application in a Fleet of Unmanned Aerial

Vehicles," *IEEE Access*, vol. 9, pp. 104940-104949, 2021, https://doi.org/10.1109/ACCESS.2021.3098303.

[15] A. Amirkhani and A. H. Barshooi, "Consensus in multi-agent systems: a review," *Artificial Intelligence Review*, vol. 55, no. 5, pp. 3897-3935, 2022, https://doi.org/10.1007/s10462-021-10097-x.

[16] A. Singha, A. K. Ray, and M. C. Govil, "Adaptive neural network based quadrotor UAV formation control under external disturbances," *Aerospace Science and Technology*, vol. 155, p. 109608, 2024, https://doi.org/10.1016/j.ast.2024.109608.

[17] N. Ma and Y. Cao, "Consensus-based distributed formation control for coordinated battle system of manned/unmanned aerial vehicles," *Transactions of the Institute of Measurement and Control*, vol. 46, no. 1, pp. 3-14, 2024, https://doi.org/10.1177/01423312231171815.

[18] J. Jia, X. Chen, W. Wang, and M. Zhang, "Event-triggered cooperative control for moving target encirclement and tracking with time-varying pattern by UAV formation," *IET Control Theory & Applications*, vol. 18, no. 1, pp. 55-70, 2024, https://doi.org/10.1049/cth2.12539.

[19] Z. A. Ali, A. Israr, E. H. Alkhammash, and M. Hadjouni, "A Leader-Follower Formation Control of Multi-UAVs via an Adaptive Hybrid Controller," *Complexity*, vol. 2021, no. 1, p. 9231636, 2021, https://doi.org/10.1155/2021/9231636.

[20] J. Gao *et al*., "Digital Battle: A Three-Layer Distributed Simulation Architecture for Heterogeneous Robot System Collaboration," *Drones*, vol. 8, no. 4, p. 156, 2024, https://doi.org/10.3390/drones8040156.

[21] I. M. Lazim, A. R. Husain, Z. Mohamed, M. A. M. Basri, N. A. M. Subha, and L. Ramli, "Disturbance observer-based formation tracking control of multiple quadrotors in the presence of disturbances," *Transactions of the Institute of Measurement and Control*, vol. 41, no. 14, pp. 4129-4141, 2019, https://doi.org/10.1177/0142331219851925.

[22] Y. Liu, Z. Liu, G. Wang, C. Yan, X. Wang, and Z. Huang, "Flexible multi-UAV formation control via integrating deep reinforcement learning and affine transformations," *Aerospace Science and Technology*, vol. 157, p. 109812, 2025, https://doi.org/10.1016/j.ast.2024.109812.

[23] C. Urrea, "Hybrid Fault-Tolerant Control in Cooperative Robotics: Advances in Resilience and Scalability," *Actuators*, vol. 14, no. 4, p. 177, 2025, https://doi.org/10.3390/act14040177.

[24] Z. Yu, Y. Zhang, B. Jiang, J. Fu, Y. Jin, "A review on fault-tolerant cooperative control of multiple unmanned aerial vehicles," *Chinese Journal of Aeronautics*, vol. 35, no. 1, pp. 1-18, 2022, https://doi.org/10.1016/j.cja.2021.04.022.

[25] Y. Zhang *et al*., "Adaptive Observer-Based Neural Network Control for Multi-UAV Systems with Predefined-Time Stability," *Drones*, vol. 9, no. 3, p. 222, 2025, https://doi.org/10.3390/drones9030222.

[26] X. Wu, T. Cao, R. Zhen, and Z. Li, "Time-Varying Formation-Containment Tracking Control for Unmanned Aerial Vehicle Swarm Systems with Switching Topologies and a Non-Cooperative Target," *Journal of Shanghai Jiaotong University (Science)*, vol. 29, no. 4, pp. 689-701, 2024, https://doi.org/10.1007/s12204-024-2728-x.

[27] A. Parvareh, M. Naderi Soorki, and A. Azizi, "The Robust Adaptive Control of Leader–Follower Formation in Mobile Robots with Dynamic Obstacle Avoidance," *Mathematics*, vol. 11, no. 20, p. 4267, 2023, https://doi.org/10.3390/math11204267.

[28] Z. Yang, M. Li, Z. Yu, Y. Cheng, G. Xu, and Y. Zhang, "Fault Detection and Fault-Tolerant Cooperative Control of Multi-UAVs under Actuator Faults, Sensor Faults, and Wind Disturbances," *Drones*, vol. 7, no. 8, p. 503, 2023, https://doi.org/10.3390/drones7080503.

[29] C. Fengmin, L. Liwei, G. Huina and F. Yan, "Event-Triggered H∞ Consensus of Leader-Follower Multi-Agent Systems Under ADT Switching Topologies," *IEEE Access*, vol. 13, pp. 118782-118792, 2025, https://doi.org/10.1109/ACCESS.2025.3586015.

[30] X. Ai, Y.-Y. Chen, and H. Yu, "Adaptive fault-tolerant formation tracking control of networked mobile robots with input delays," *Journal of the Franklin Institute*, vol. 361, no. 1, pp. 248-264, 2024, https://doi.org/10.1016/j.jfranklin.2023.11.020.

[31] P. Yue *et al*., "UAV Autonomous Navigation System Based on Air–Ground Collaboration in GPS-Denied Environments," *Drones*, vol. 9, no. 6, p. 442, 2025, https://doi.org/10.3390/drones9060442.

[32] L. Deng, Z. Shu, and T. Chen, "Event-Triggered Robust Distributed MPC for Multi-Agent Systems with A Two-Step Event Verification," *IFAC-PapersOnLine*, vol. 55, no. 34, pp. 144-149, 2022, https://doi.org/10.1016/j.ifacol.2022.11.322.

[33] X. Chang, Y. Yang, Z. Zhang, J. Jiao, H. Cheng, and W. Fu, "Consensus-Based Formation Control for Heterogeneous Multi-Agent Systems in Complex Environments," *Drones*, vol. 9, no. 3, p. 175, 2025, https://doi.org/10.3390/drones9030175.

[34] C. Liu, S. Sun, C. Tao, Y. Shou, and B. Xu, "Sliding mode control of multi-agent system with application to UAV air combat," *Computers & Electrical Engineering*, vol. 96, p. 107491, 2021, https://doi.org/10.1016/j.compeleceng.2021.107491.

[35] L. Cheng, X. Chen, F. Zhao, J. Qiu, and J. Cao, "Observer-Based Prescribed-Time Leader-Follower Consensus for Nonlinear Multiagent Systems Under Stochastic Switching Topologies," *Journal of Systems Science and Complexity*, vol. 38, no. 4, pp. 1595-1613, 2025, https://doi.org/10.1007/s11424-025-4355-5.

[36] G. Hu, Y. Zhu, D. Zhao, M. Zhao and J. Hao, "Event-Triggered Communication Network With Limited-Bandwidth Constraint for Multi-Agent Reinforcement Learning," *IEEE Transactions on Neural Networks and Learning Systems*, vol. 34, no. 8, pp. 3966-3978, 2023, https://doi.org/10.1109/TNNLS.2021.3121546.

[37] Z. Ma, H. Gong, and X. Wang, "Formation fault-tolerant control for multiple UAVs with external disturbances," *Aircraft Engineering and Aerospace Technology*, vol. 96, no. 3, pp. 403-416, 2024, https://doi.org/10.1108/AEAT-05-2023-0148.

[38] Y. Huang, "Adaptive consensus for uncertain multi-agent systems with stochastic measurement noises," *Communications in Nonlinear Science and Numerical Simulation*, vol. 120, p. 107156, 2023, https://doi.org/10.1016/j.cnsns.2023.107156.

[39] Y. Chen and Z. Li, "Formation adaptation in obstacle-cluttered environments via MPC-based trajectory planning," *Science China Information Sciences*, vol. 67, no. 7, p. 174201, 2024, https://doi.org/10.1007/s11432-023-4031-y.

[40] X. Chen and H. Chen, "Event-Triggered Time-Varying Formation Tracking Control for Multi-Agent Systems with a Switching-Directed Topology," *Mathematics*, vol. 11, no. 20, p. 4245, 2023, https://doi.org/10.3390/math11204245.

[41] Z. Wang, M. Chadli, and S. X. Ding, "A dynamic event-triggered approach for observer-based formation control of multi-agent systems with designable inter-event time," *Systems & Control Letters*, vol. 195, p. 105970, 2025, https://doi.org/10.1016/j.sysconle.2024.105970.

[42] W. Cai, Y. Ju, Z. Liu, M. Zhang, and S. Lv, "Event-triggered leader-follower communication based formation control with dual-predictor for multiple AUVs," *Ocean Engineering*, vol. 334, p. 121552, 2025, https://doi.org/10.1016/j.oceaneng.2025.121552.

[43] X. Lv, C. Peng, and J. Ma, "Control Barrier Function-Based Collision Avoidance Guidance Strategy for Multi-Fixed-Wing UAV Pursuit-Evasion Environment," *Drones*, vol. 8, no. 8, p. 415, 2024, https://doi.org/10.3390/drones8080415.

[44] W. Wang, X. Chen, J. Jia, K. Wu, and M. Xie, "Optimal formation tracking control based on reinforcement learning for multi-UAV systems," *Control Engineering Practice*, vol. 141, p. 105735, 2023, https://doi.org/10.1016/j.conengprac.2023.105735.

[45] B. An, B. Wang, H. Fan, L. Liu, and Y. Wang, "Adaptive observer-based event-triggered finite time formation tracking for multi-agent systems with a non-cooperative leader," *Journal of the Franklin Institute*, vol. 360, no. 13, pp. 10195-10226, 2023, https://doi.org/10.1016/j.jfranklin.2023.07.013.

[46] J. Li, J. Xi, M. He, and B. Li, "Formation control for networked multiagent systems with a minimum energy constraint," *Chinese Journal of Aeronautics*, vol. 36, no. 1, pp. 342-355, 2023, https://doi.org/10.1016/j.cja.2022.01.015.

[47] L. Ma, D. Meng, X. Huang and S. Zhao, "Vision-Based Formation Control for an Outdoor UAV Swarm With Hierarchical Architecture," *IEEE Access*, vol. 11, pp. 75134-75151, 2023, https://doi.org/10.1109/ACCESS.2023.3296603.

[48] C. Jiang, X. Huang, and Y. Guo, "End-to-end decentralized formation control using a graph neural network-based learning method," *Frontiers in Robotics and AI*, vol. 10, p. 1285412, 2023, https://doi.org/10.3389/frobt.2023.1285412.

[49] H. Yancai, L. Yang, Z. Yan, and D. T. Minh Hoang, "Adaptive formation control for obstacle avoidance of USVs with asymmetric input saturation," *Scientific Reports*, vol. 14, no. 1, p. 22515, 2024, https://doi.org/10.1038/s41598-024-73560-z.

[50] Y. Zhu, S. Li, G. Guo, P. Yuan, and J. Bai, "Formation control of UAV–USV based on distributed event-triggered adaptive MPC with virtual trajectory restriction," *Ocean Engineering*, vol. 294, p. 116850, 2024, https://doi.org/10.1016/j.oceaneng.2024.116850.

[51] F. Zhang, K. Gu and Y. Shen, "Vision-Based Localization in Multi-Agent Networks With Communication Constraints," *IEEE Transactions on Vehicular Technology*, vol. 71, no. 1, pp. 518-532, 2022, https://doi.org/10.1109/TVT.2021.3128492.

[52] Z. Pan, J. Feng, T. Yu, B. Cui and Y. Xia, "Distributed Recursive Grouping-Based Fault Self-Healing of UAV Swarm With Individuals Failure," *IEEE Transactions on Aerospace and Electronic Systems*, vol. 61, no. 2, pp. 2996-3008, 2025, https://doi.org/10.1109/TAES.2024.3480050.

[53] B. Liu, A. Li, Y. Guo, and C. Wang, "Distributed finite-time backstepping adaptive containment control for multiple unmanned aerial vehicles with input saturation," *International Journal of Robust and Nonlinear Control*, vol. 34, no. 12, pp. 7837-7858, 2024, https://doi.org/10.1002/rnc.7368.

[54] N. Li, P. Borja, J. M. A. Scherpen, A. van der Schaft and R. Mahony, "Passivity-Based Trajectory Tracking and Formation Control of Nonholonomic Wheeled Robots Without Velocity Measurements," *IEEE Transactions on Automatic Control*, vol. 68, no. 12, pp. 7951-7957, 2023, https://doi.org/10.1109/TAC.2023.3258320.

[55] M. Xu, Y. Fang, J. Li, and X. Zhao, "Finite Time Fully Distributed Consensus Control for Multi-agent System With Input Saturation and Limited Communication Resources," *International Journal of Control, Automation and Systems*, vol. 21, no. 11, pp. 3659-3672, 2023, https://doi.org/10.1007/s12555-022-0480-2.

[56] Z. Liu and Y. Liu, "Compensation Observer-Based Adaptive Output Feedback Control for Multi-Agent Systems," *Applied Sciences*, vol. 14, no. 13, p. 5406, 2024, https://doi.org/10.3390/app14135406.

[57] Z. Xiong, Z. Liu, Y. Luo, and J. Xia, "An Adaptive and Bounded Controller for Formation Control of Multi-Agent Systems with Communication Break," *Applied Sciences*, vol. 12, no. 11, p. 5602, 2022, https://doi.org/10.3390/app12115602.

[58] D. Yao, H. Li, R. Lu, and Y. Shi, "Event-based distributed sliding mode formation control of multi-agent systems and its applications to robot manipulators," *Information Sciences*, vol. 614, pp. 87-103, 2022, https://doi.org/10.1016/j.ins.2022.09.059.

[59] J. Xie *et al*., "Reinforcement-Learning-Based Asynchronous Formation Control Scheme for Multiple Unmanned Surface Vehicles," *Applied Sciences*, vol. 11, no. 2, p. 546, 2021, https://doi.org/10.3390/app11020546.

[60] I. B. Ghiloubi, L. Abdou, and O. Lahmar, "Adjusted linear quadratic regulator-proportional-derivative control of Quanser's three degrees of freedom helicopter based on flower pollination algorithm under external disturbances," *IAES International Journal of Robotics and Automation (IJRA)*, vol. 13, no. 4, pp. 432-444, 2024, http://doi.org/10.11591/ijra.v13i4.pp432-444.

[61] S. Obukhov, E. M. Ahmed, D. Y. Davydov, T. Alharbi, A. Ibrahim, and Z. M. Ali, "Modeling wind speed based on fractional ornstein-uhlenbeck process," *Energies*, vol. 14, no. 17, p. 5561, 2021, https://doi.org/10.3390/en14175561.